Supplementary Information (SI) for Journal of Materials Chemistry A.
This journal is © The Royal Society of Chemistry 2026
Supplementary Information (SI) for Journal of Materials Chemistry A.
This journal is © The Royal Society of Chemistry 2025

# Electronic Supporting Information

## A Novel Bipolar Phthalocyanine-Based Composite Cathode for Advanced Zn-Organic Batteries

Ruiqi Ye,[a] Fuxin Zhu,[a] Qinxin Zhou,[b] Feng Qiu*[b] and Ping Li*[a]

[a] School of Chemistry and Chemical Engineering, Chongqing University of Science and Technology, Chongqing, 401331, P.R. China.

E-mail: liping@cqust.edu.cn; 2020020@cqust.edu.cn

[b] School of Materials and New Energy, Chongqing University of Science and Technology, Chongqing, 401331, P.R. China.

E-mail: qiufeng@cqust.edu.cn

# Table of Contents

**Fig. S14** Cyclic voltammograms of the CuPc-DPTZ-CMPs/CNT composite in 3 M $Zn(CF_3SO_3)_2$ aqueous electrolyte are shown at different scan rates: (a) 2 to 10 mV $s^{-1}$ and (b) 20 to 100 mV $s^{-1}$.

**Fig. S15** The linear relation between the b value and the three sweep regions (0.2–1.0, 2–10, 20–100 mV $s^{-1}$) of the cathodic and anodic peaks.

**Fig. S16** Cyclic voltammetry profiles of CuPc-DPTZ-CMPs/CNT composite in different electrolytes at the scan rate 10 mV $s^{-1}$.

**Fig. S17** GCD curves of CuPc-DPTZ-CMPs/CNT composite in different electrolytes.

**Fig. S18** Ex situ FT-IR spectra of CuPc-DPTZ-CMPs/CNT composite cathode at the pristine and (dis)charge states.

**Fig. S19** SEM images and EDS-mapping of C, N and Cu element distributions on CuPc-DPTZ-CMPs/CNT composite electrodes at different states.

**Fig. S20** Ex situ XPS spectra of Cu 2p at the pristine and (dis)charge states.

**Fig. S21** Ex situ XRD patterns of CuPc-DPTZ-CMPs/CNT composite cathode at the pristine and (dis)charge states.

## References

## Section S1 Experimental Procedures and Calculated Methods

### 1.1 Materials

Unless otherwise stated, all chemicals are commercially available and are used as received. (Tetraaminophthalocyaninato)copper(II) ($CuPc(NH_2)_4$), Carboxylic Multi-walled Carbon Nanotubes (CNT), Tetrahydrofuran (THF), Sodium tert-butoxide (NaOtBu), Potassium bromide (KBr), Mesitylene ($C_9H_{12}$),1,4-Dioxane ($C_4H_8O_2$), Trifluoromethanesulfonic acid zinc salt ($Zn(CF_3SO_3)_2$), Trifluoromethanesulfonic acid and 2-Dicyclohexylphosphino-2',4',6'-triisopropylbiphenyl (X-Phos) were purchased from Macklin Chemical Industry Co. 3,7-dibromo-10H-phenothiazine and Bis(dibenzylideneacetone)palladium ($Pd(dba)_2$) were purchased from Bidepharm. Acetonitrile (ACN) was purchased from Aladdin.

### 1.2 Synthesis of CuPc-DPTZ-CMPs/CNT composite

A 15 mL Pyrex tube charged with 63.6 mg $CuPc(NH_2)_4$ (0.1 mmol), 85.68 mg DPTZ (0.24 mmol), CNT (40 mg), 5.77 mg $Pd(dba)_2$ (0.01 mmol), 7.17 mg X-Phos (0.015 mmol), 11.9 mg KBr (0.1 mmol), 38.5 mg NaOtBu (0.4 mmol), 1,4-dioxane (1 mL) and mesitylene (1 mL) was treated by sonication for 1 h. Subsequently, the mixture was rapidly frozen using liquid nitrogen. The mixture was degassed by three freeze-pump-thaw cycles, purged with $N_2$, and stirred at 120 °C for 5 days. After the reaction was cooled to room temperature, distilled water was added, and the mixture was stirred for 1 hour, then filtered and sequentially washed with distilled water, tetrahydrofuran, and acetone. Then, Soxhlet extraction was performed with acetone to remove the unreacted monomer, and the obtained product was vacuum dried for 24 h, yielding 0.135 g of a black-green powder with a yield of 92%. Similarly, CuPc-DPTZ CMPs was synthesized without adding CNT. The resulting product was vacuum dried for 24 hours, yielding 0.094 g of a deep green powder with a yield of 94%.

### 1.3 Electrochemical measurements

For aqueous zinc-organic battery (ZOBs), the electrode was prepared by mixing active material (CuPc-DPTZ-CMPs/CNT composite, CuPc-DPTZ CMPs or CNT), carbon black, and Poly tetra fluoro ethylene (PTFE) in a weight ratio of 5:4:1. Then the slurry was uniformly coated onto stainless steel nets or carbon cloth and dried at 60 ℃ for 24 h. The load of the cathode material is 0.39-0.70 mg $cm^{-2}$. The prepared carbon cloth, whose surface is coated with CuPc-DPTZ-CMPs/CNT composite, CuPc-DPTZ CMPs, or CNT slurry, is employed as the positive electrode of the battery; the zinc

sheet is utilised as the negative electrode, and the 3 M $Zn(CF_3SO_3)_2$ aqueous solution is utilised as the electrolyte to assemble the battery. Cyclic voltammetry (CV), galvanostatic charge/discharge (GCD), electrochemical impedance spectroscopy (EIS), and cyclic stability tests were conducted on a CHI760E electrochemical workstation within the voltage range of 0.6–1.7 V. For the electrochemical test of $H^+$ and $Zn^{2+}$ insertion capacity, three electrodes were used, with a stainless steel mesh coated with CuPc-DPTZ-CMPs/CNT composite paste as the working electrode, a platinum electrode as the counter electrode, and a saturated Ag/AgCl electrode as the reference electrode, with 3 M $Zn(CF_3SO_3)_2/H_2O$ electrolyte, 0.2 M $Zn(CF_3SO_3)_2$/acetonitrile (ACN) non-aqueous electrolyte and 0.635 mM $CF_3SO_3H/H_2O$ electrolyte, respectively. These measurements were conducted using three distinct three-electrode systems as described above. The specific capacity ($C_m$, mAh $g^{-1}$) is calculated from the GCD curve according to the following equation:

$$C_m = \frac{\int_0^{\Delta t} i \times dt}{m} \quad \text{(Eq. S1)}$$

In this context, $C_m$ represents the specific capacity of the battery (mAh $g^{-1}$), i denotes the magnitude of the current employed in the test (mA), m signifies the mass of the active material of the working electrode (g), and Δt denotes the discharge time (h).

The gravimetric energy density (E, Wh $kg^{-1}$) of Zn//CuPc-DPTZ-CMPs/CNT composite battery was estimated based on the following equation:

$$E = C_m \times \Delta V \quad \text{(Eq. S2)}$$

where $\Delta V$ denotes the average discharge voltage. The energy density was estimated based on the mass loading of active organic materials in the cathodes[S1].

**1.4 Charge storage kinetics calculations**

The capacitive effect of the battery can be evaluated through the analysis of the CV results obtained at varying scan rates. In general, the relationship between the peak current ($i$) and the sweep rate ($v$) in the CV can be described by the following equation:

$$i = av^b \quad \text{(Eq. S3)}$$

$$\log(i) = b\log(v) + \log(a) \quad \text{(Eq. S4)}$$

In this context, the tunable parameters a and b are of particular interest. The value of b determines the insertion/extraction behaviour of $Zn^{2+}$ during redox processes. Values of b equal to 0.5 and 1.0 indicate diffusion control behaviour and capacitance control behaviour, respectively[S2].

The contribution of pseudo-capacitance and diffusion-controlled charge storage can be quantified further by employing the following formula:

$$i(E) = K_1 v + K_2 v^{1/2} \quad \text{(Eq. S5)}$$

In this context, the symbols i(E), $k_1v$, and $k_2v^{1/2}$ are used to represent the total current response at relative potential (E), the current resulting from the capacitive-controlled reaction, and the current resulting from the diffusion-controlled reaction, respectively[S3–S5]. Consequently, the relative contribution of the pseudo-capacitance and diffusion control processes can be calculated at a fixed potential. The preceding equation should be rewritten as follows:

$$\frac{i(E)}{v^{1/2}} = k_1 v^{1/2} + k_2 \quad \text{(Eq. S6)}$$

**1.5 Characterization**

Fourier transform infrared spectroscopy (FT-IR) was conducted on a NICOLET iS10 spectrometer with a reflection mode within the wavenumber range of 4000 to 500 $cm^{-1}$. Ultraviolet-visible-near infrared spectrophotometer (UV-vis-NIR spectrophotometer, UH5700, Hitachi, Tokyo, Japan) within the range of 200-1200 nm. X-ray diffraction tests were conducted using X-ray diffraction (XRD, XRD-7000 with Cu Kα radiation source, Shimadzu Corporation of Japan) for the purpose of analysing the material structure. The sample morphology was observed by field-emission scanning electron microscopy (SEM, S-4800, Hitachi) and transmission electron microscopy (TEM, Talos F200S, Thermo Scientific). The porous structures of CuPc-DPTZ CMPs and CuPc-DPTZ-CMPs/CNT composite were analyzed using $N_2$ (at 77 K) adsorption/desorption from Micromeritics ASAP 2460, with the specific surface area of the samples (CuPc-DPTZ CMPs and their composite) being determined. The Brunauer-Emmett-Teller (BET) method was employed to calculate the specific surface area, while the Non-Local Density Functional Theory (NLDFT) was used to determine the pore size distribution from the adsorption branch. The ultraviolet-visible (UV-vis) spectra were obtained with a MAPADA-M9 UV-vis spectrometer. X-ray photoelectron spectroscopy (XPS, Thermo Scientific K-Alpha, United States) was employed to investigate the chemical interactions between charge carriers and the surface functional groups of electrodes (i.e., electroactive materials), thereby elucidating the charge storage mechanisms.

## Section S2 Supporting Characterizations

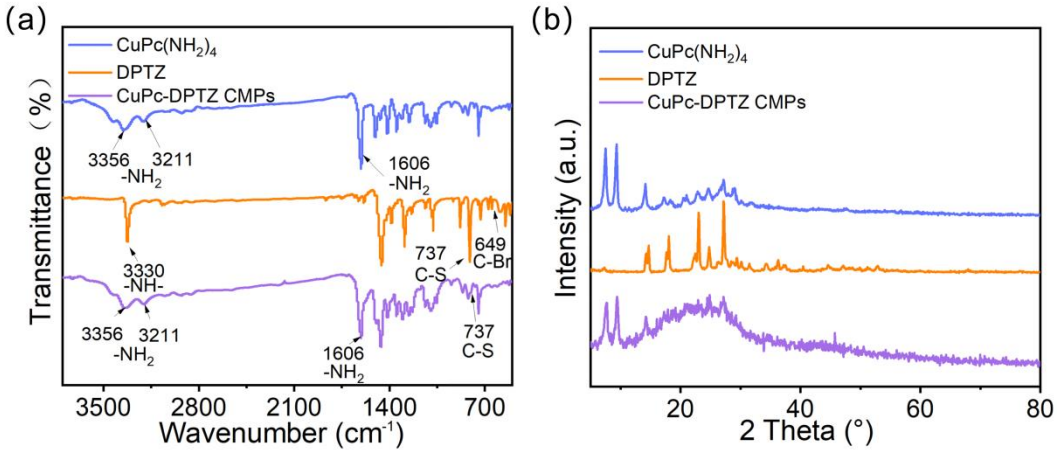


**Fig. S1** (a) FT-IR spectra of $CuPc(NH_2)_4$, DPTZ and CuPc-DPTZ CMPs. (b) XRD patterns of $CuPc(NH_2)_4$, DPTZ and CuPc-DPTZ CMPs.

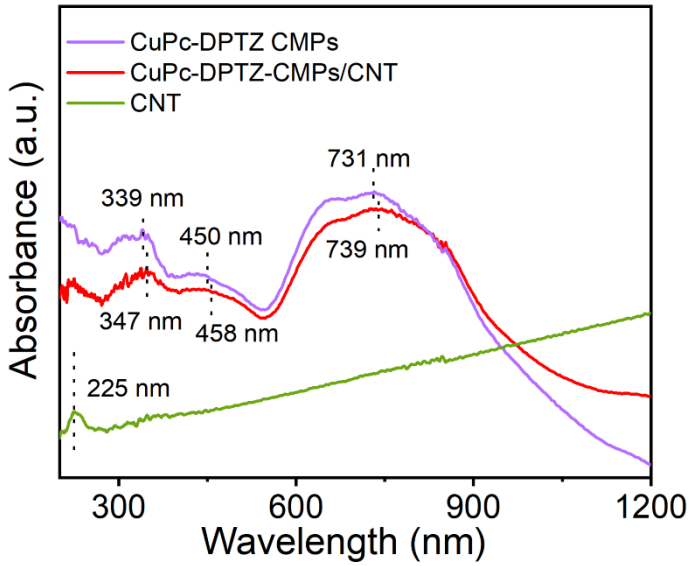


**Fig. S2** UV-vis-NIR spectra of CuPc-DPTZ CMPs, CuPc-DPTZ CMPs/CNT composite and CNT.

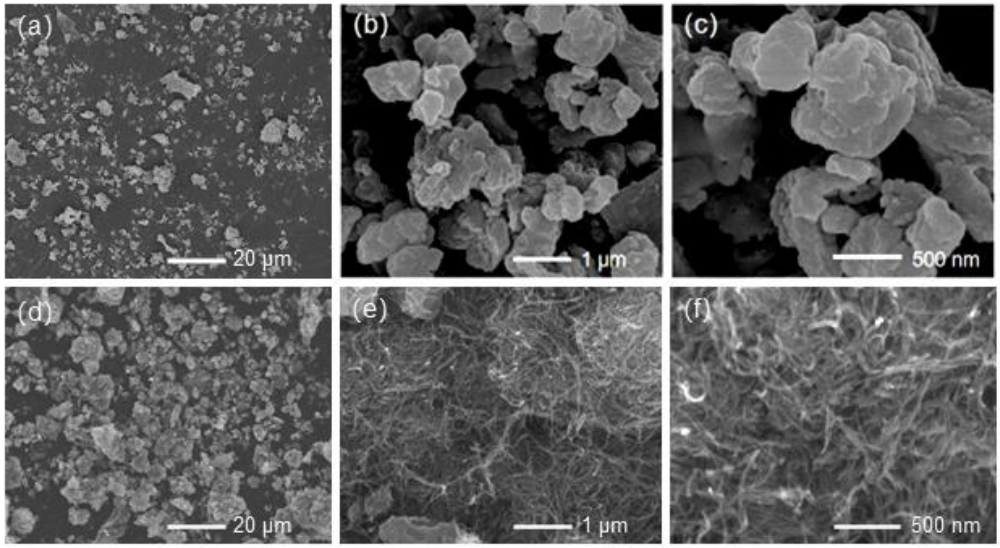


**Fig. S3** SEM images of (a-c) CuPc-DPTZ CMPs and (d-f) CuPc-DPTZ-CMPs/CNT composite.

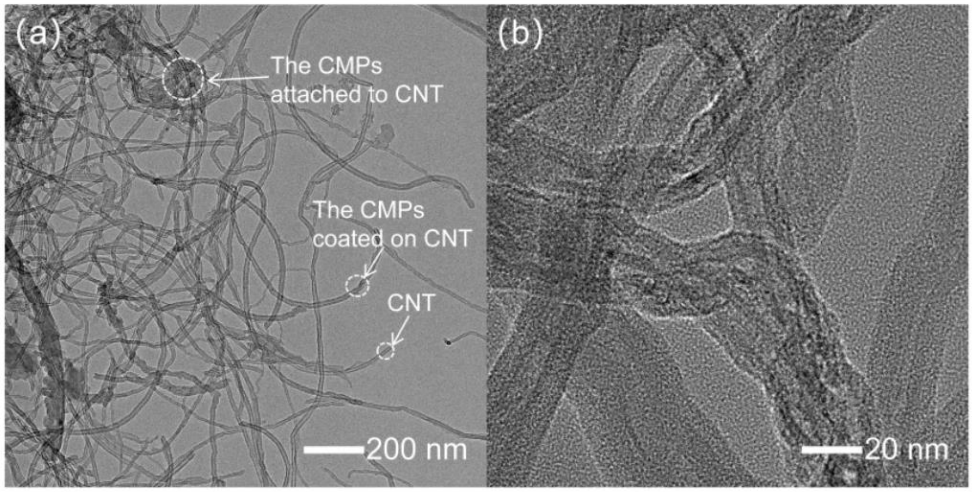


**Fig. S4** (a) TEM and (b) HR-TEM image of CuPc-DPTZ-CMPs/CNT composite.

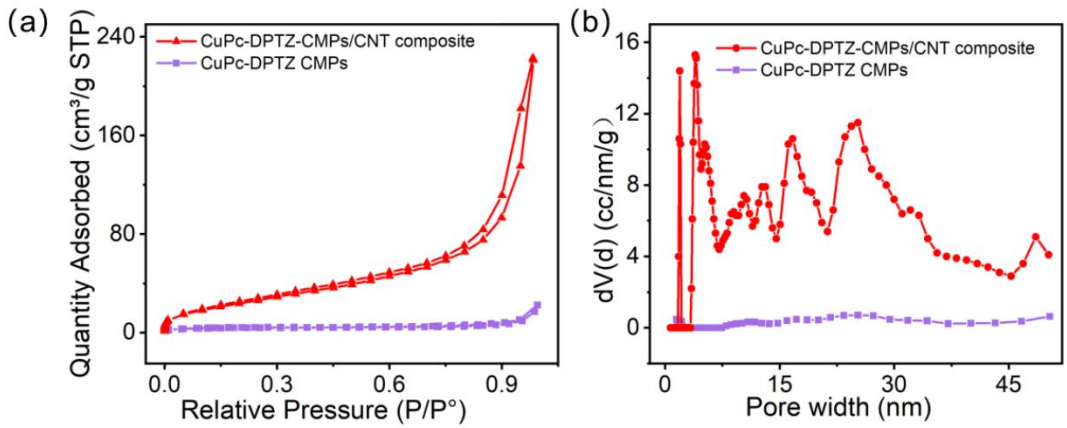


**Fig. S5** (a) $N_2$ adsorption-desorption isotherms and (b) the corresponding pore size distribution of CuPc-DPTZ CMPs and CuPc-DPTZ-CMPs/CNT composite.

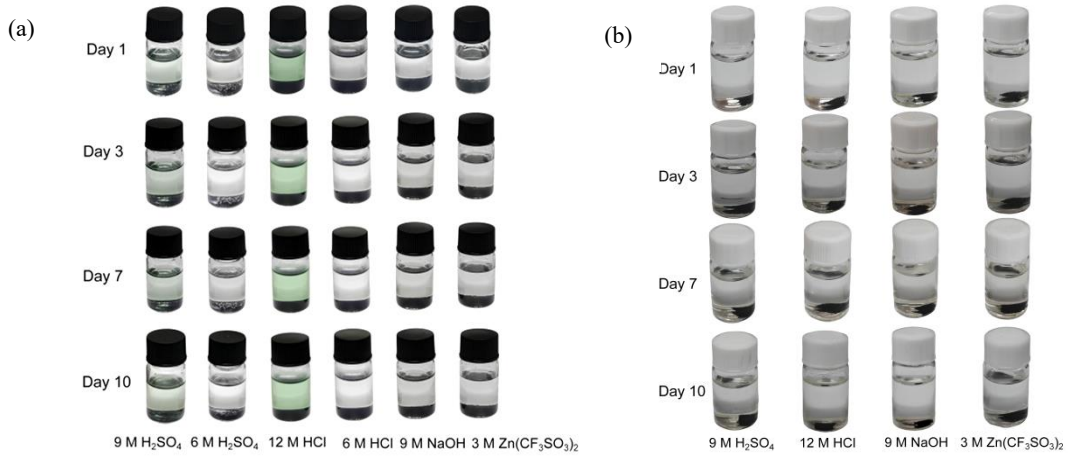


**Fig. S6** Digital photographs showing the color evolution of the CuPc-DPTZ-CMPs/CNT composite in various solutions over time: (a) powder and (b) electrode sheet, immersed in acid/base solutions of different concentrations and the practical 3 M $Zn(CF_3SO_3)_2$ aqueous electrolyte at specified time intervals, respectively.

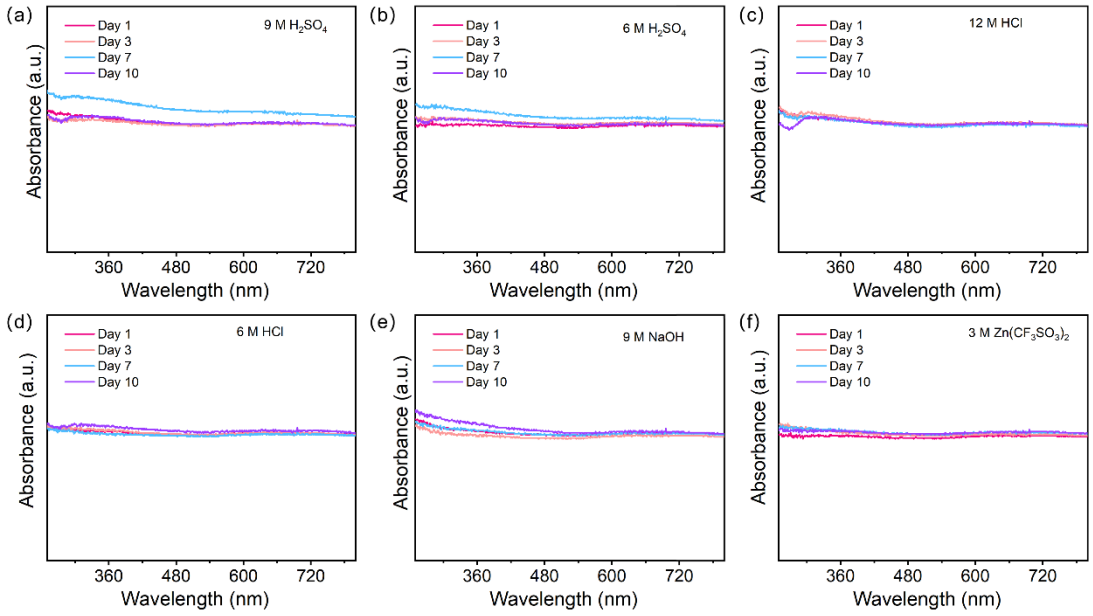


**Fig. S7** The UV-vis absorption spectra of the CuPc-DPTZ-CMPs/CNT composite powder over time (1, 3, 7, and 10 days) in different solutions: (a) 9 M $H_2SO_4$, (b) 6 M $H_2SO_4$, (c) 12 M HCl, (d) 6 M HCl, (e) 9 M NaOH, and (f) 3 M $Zn(CF_3SO_3)_2$.

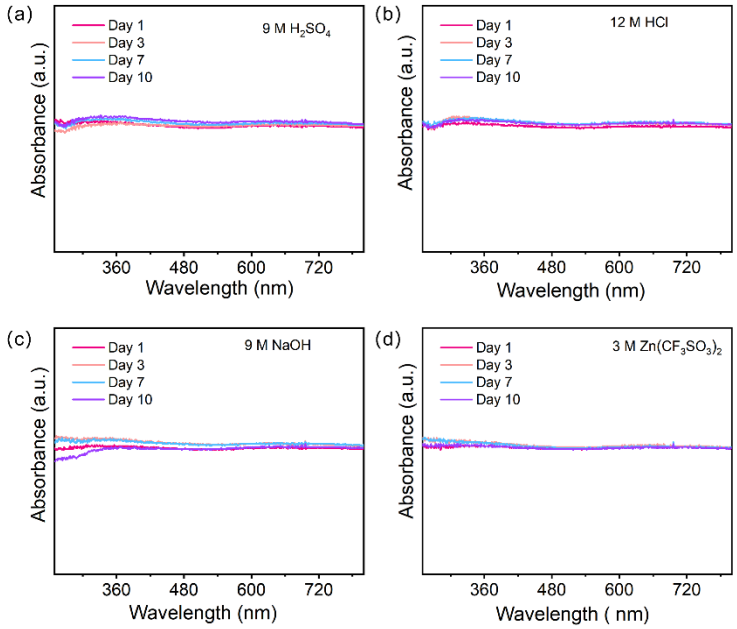


**Fig. S8** The UV-vis absorption spectra of the CuPc-DPTZ-CMPs/CNT composite electrode over time (1, 3, 7, and 10 days) in different solutions: (a) 9 M $H_2SO_4$, (b) 12 M HCl, (c) 9 M NaOH, and (d) 3 M $Zn(CF_3SO_3)_2$.

To systematically assess the chemical stability of the CuPc-DPTZ-CMPs/CNT composite, dissolution tests were conducted on both the powder and the fabricated electrode sheets. The dissolution behavior of the material in concentrated acids, concentrated alkali, and 3 M $Zn(CF_3SO_3)_2$ electrolyte was systematically investigated by continuously monitoring solution color changes over a period of 1 to 10 days, combined with UV-vis absorption spectroscopy. As shown in Fig. S5, S6, and S7, the powder remained stable in 6 M $H_2SO_4$, 6 M HCl, 9 M NaOH, and 3 M $Zn(CF_3SO_3)_2$ electrolyte: no change in solution color was observed, and no characteristic absorption peaks were detected in the UV-vis spectra. In contrast, under more extreme acidic conditions (9 M $H_2SO_4$ and 12 M HCl), slight color changes occurred, and weak characteristic absorption peaks appeared in the UV-vis spectra, indicating minimal dissolution of the powder. Notably, when the CuPc-DPTZ-CMPs/CNT composite was fabricated into electrode sheets, no color change or characteristic absorption peaks were observed even in 9 M $H_2SO_4$ and 12 M HCl, demonstrating significantly enhanced stability upon electrode fabrication. These results confirm that the composite exhibits excellent chemical stability, which is markedly improved in the electrode form—a critical attribute enabling superior long-term cycling performance.

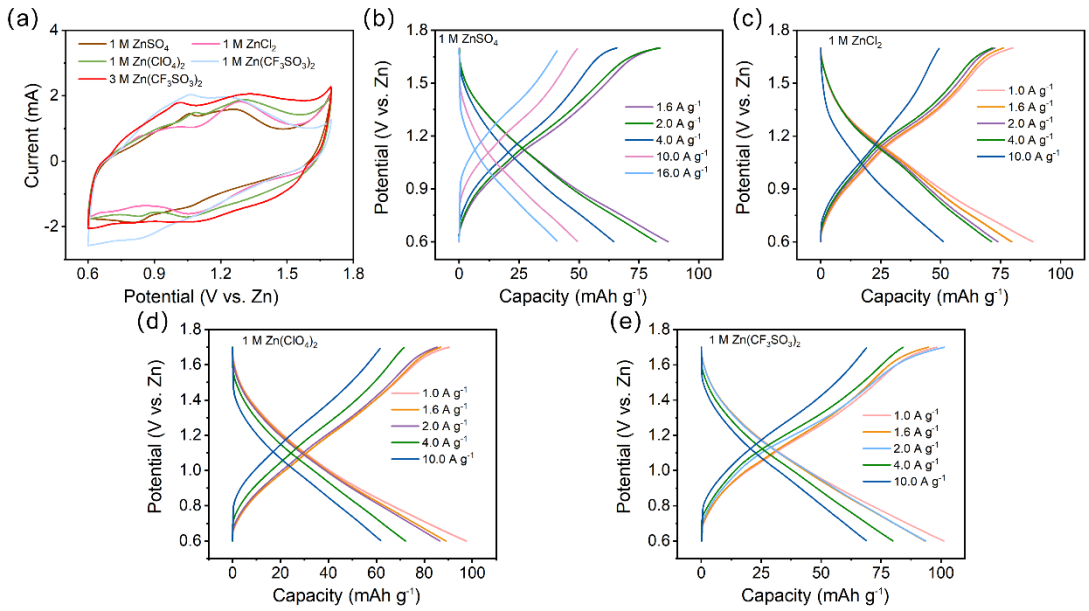


**Fig. S9** (a) Cyclic voltammetry profiles of CuPc-DPTZ-CMPs/CNT composite in various electrolytes at the scan rate 10 mV $s^{-1}$. (b-e) GCD curves of CuPc-DPTZ-CMPs/CNT composite in different electrolytes.

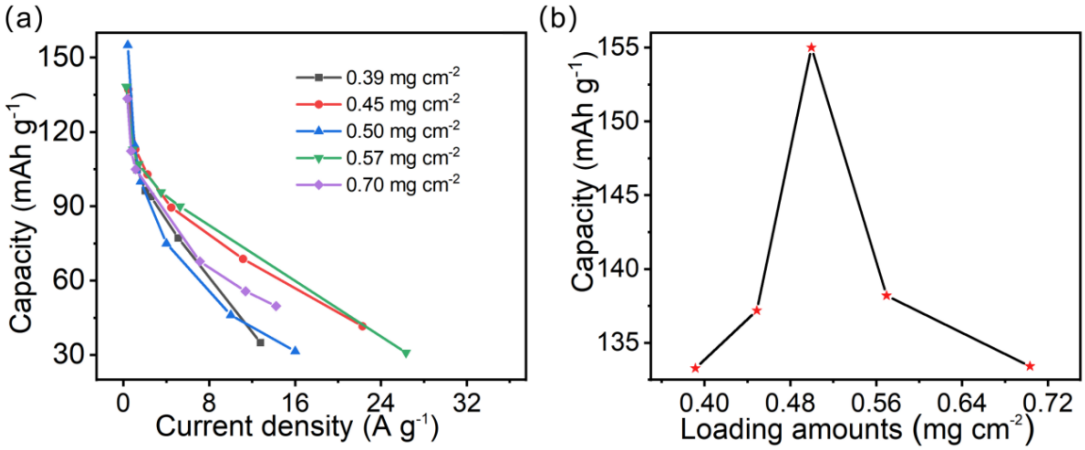


**Fig. S10** (a) Capacity-current density plot and (b) capacity-loading amounts plot for CuPc-DPTZ-CMPs/CNT composite.

**Table S1.** Summary of the electrochemical properties of representative bipolar organic electrode materials.

| | Cathode | Redox Groups | Specific Capacity (mAh $g^{-1}$) | Average discharge voltage (V) | E (Wh $kg^{-1}$) | Ref. |
|---|---|---|---|---|---|---|
| 1 | PDAN | C=N<br>-NH- | 140.0 at 0.1 A $g^{-1}$ | 0.87 | 121.1 | [S6] |
| 2 | PTD-1 | C=S<br>C=N<br>-NH- | 188.2 at 0.04 A $g^{-1}$ | 1.10 | 207.0 | [S7] |
| 3 | PDB | C=O<br>C−S | 205.0 at 0.05 A $g^{-1}$ | 0.93 | 190.1 | [S8] |
| 4 | TNP | $NO_2$<br>-NH- | 338.0 at 0.2 A $g^{-1}$ | 1.08 | 365.0 | [S9] |
| 5 | PTDM | C=N<br>-NH-<br>C=S | 118.3 at 0.1 A $g^{-1}$ | 1.13 | 99.0 | [S10] |
| 6 | PONEA/GO | C=O<br>-NH- | 329.0 at 0.1 A $g^{-1}$ | 0.74 | 242.0 | [S11] |

| | | | | | | |
|---|---|---|---|---|---|---|
| 7 | PANI | C=N<br>-NH- | 200.0 at 0.05 A $g^{-1}$ | 1.10 | 220.0 | [S12] |
| 8 | AOS | C=N<br>C-N | 465.0 at 0.1 A $g^{-1}$ | ~1.00 | 412.0 | [S13] |
| 9 | CMP | C=O<br>-NH- | 125.0 at 0.2 A $g^{-1}$ | 0.39 | 49.0 | [S14] |
| 10 | rGO@CMP | C=O<br>-NH- | 378.0 at 0.2 A $g^{-1}$ | 0.66 | 251.0 | [S14] |
| 11 | IDT | C=O<br>-NH- | 238.0 at 0.2 A $g^{-1}$ | 0.67 | 159.1 | [S15] |
| 12 | QA | C=O<br>-NH- | 212.0 at 0.2 A $g^{-1}$ | 0.76 | 161.0 | [S16] |
| 13 | DHHAP | C=N<br>-NH- | 507.0 at 0.05 A $g^{-1}$ | ~0.80 | 385.0 | [S17] |
| 14 | DHTAP-2F | C=N<br>-NH- | 306.0 at 0.1 A $g^{-1}$ | 0.7 | 214.2 | [S18] |
| 15 | PCTB | C=O<br>-S- | 136.0 at 0.05 A $g^{-1}$ | 1.02 | 138.7 | [S19] |
| 16 | CuPc-DPTZ-CMPs/CNT composite | C=N<br>-NH-<br>C-S | 155.0 at 0.4 A $g^{-1}$ | 1.16 | 179.8 | **This work** |

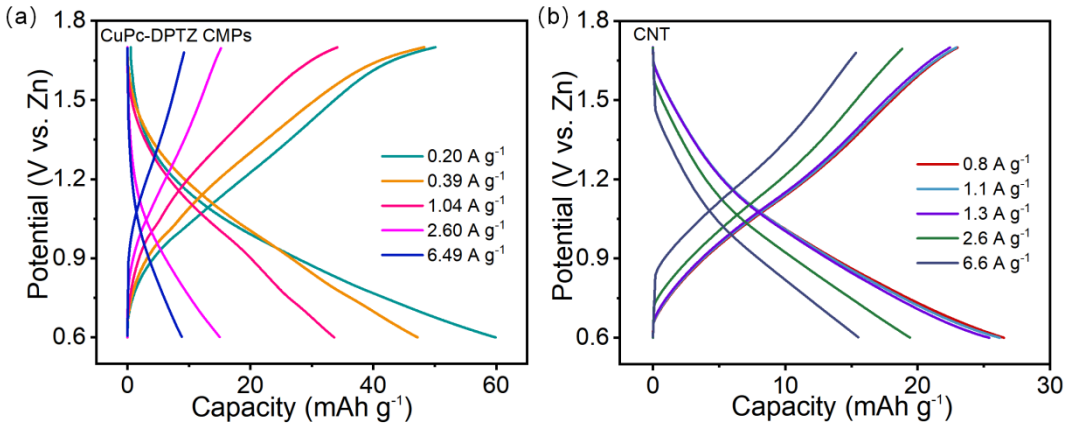


**Fig. S11** GCD curves of (a) CuPc-DPTZ CMPs and (b) CNT at different current densities.

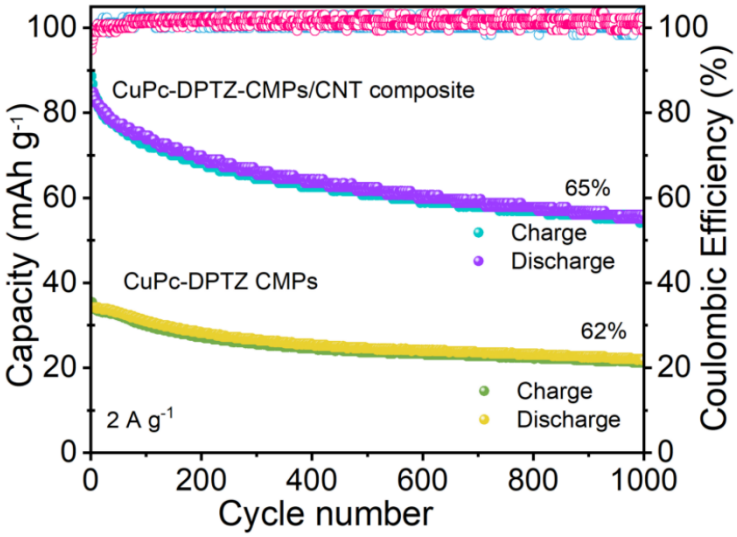


**Fig. S12** Cycling performances of CuPc-DPTZ CMPs and CuPc-DPTZ-CMPs/CNT composite at a current density of 2 A $g^{-1}$.

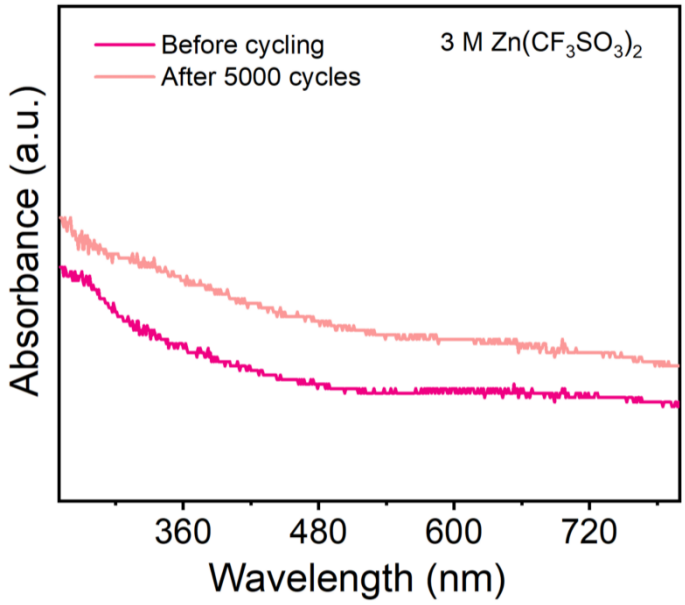


**Fig. S13** The UV-vis absorption spectra of the 3 M $Zn(CF_3SO_3)_2$ electrolyte before and after 5000 cycles.

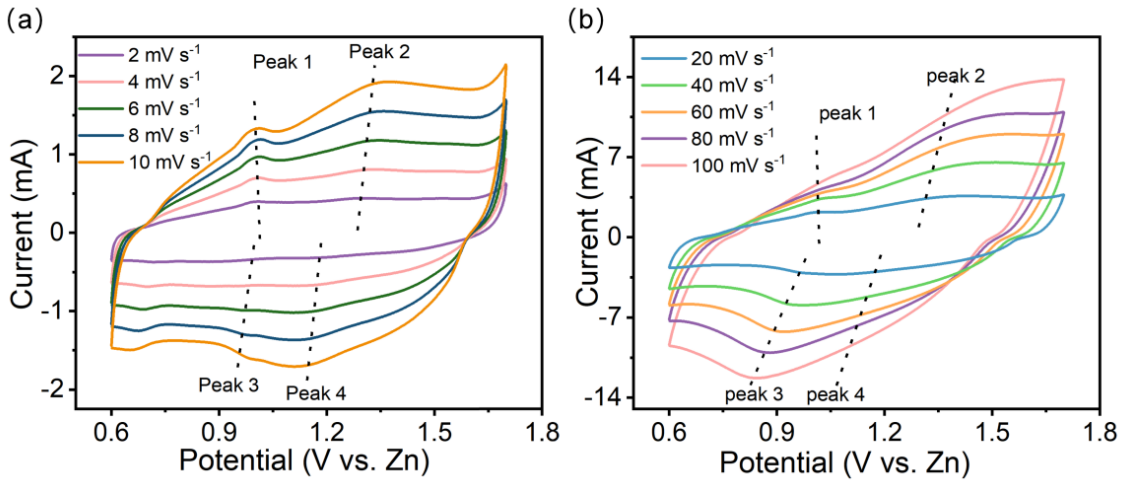


**Fig. S14** Cyclic voltammograms of the CuPc-DPTZ-CMPs/CNT composite in 3 M $Zn(CF_3SO_3)_2$ aqueous electrolyte are shown at different scan rates: (a) 2 to 10 mV $s^{-1}$ and (b) 20 to 100 mV $s^{-1}$.

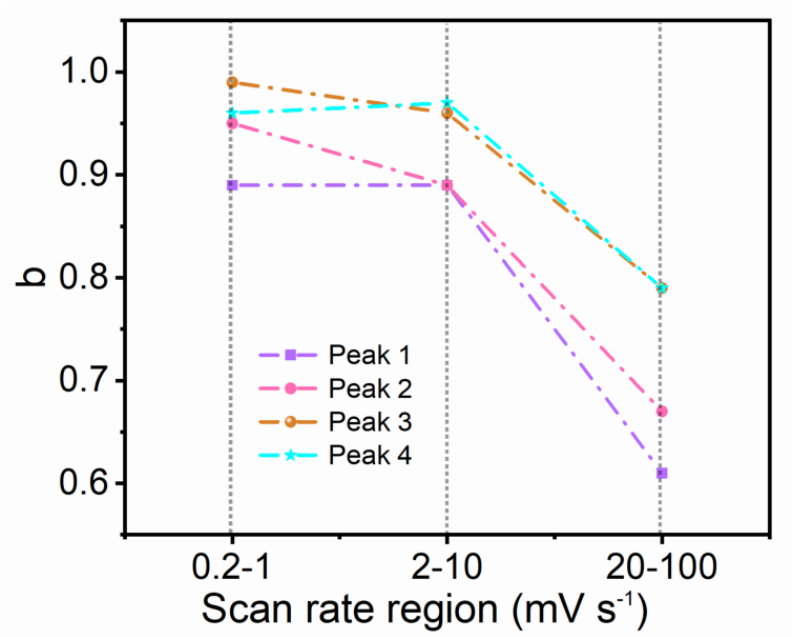


**Fig. S15** The linear relation between the b value and the three sweep regions (0.2–1.0, 2–10, 20–100 mV $s^{-1}$) of the cathodic and anodic peaks.

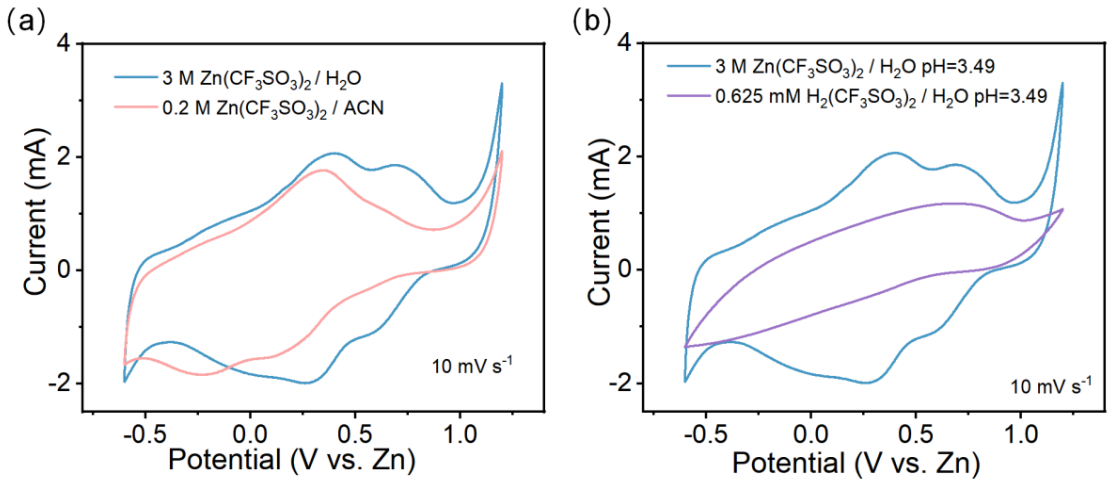


**Fig. S16** Cyclic voltammetry profiles of CuPc-DPTZ-CMPs/CNT composite in different electrolytes at the scan rate 10 mV $s^{-1}$.

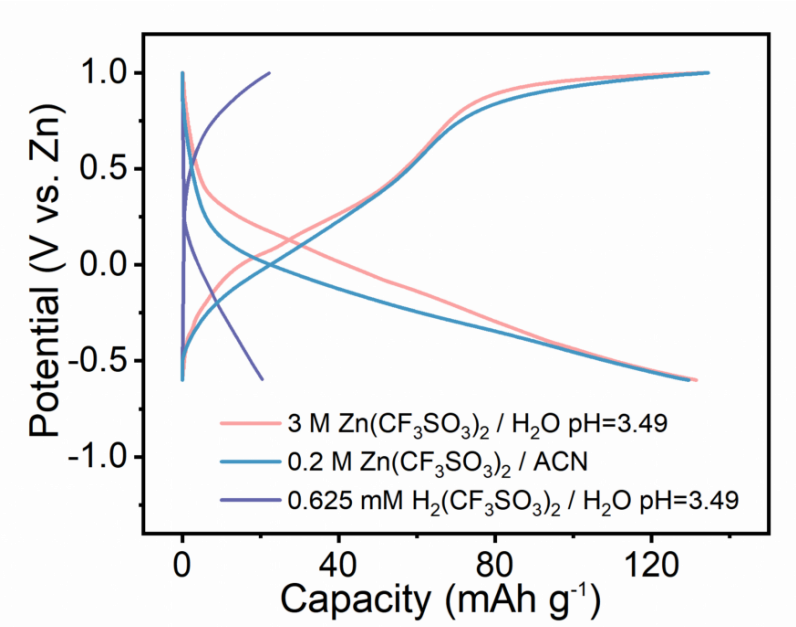


**Fig. S17** GCD curves of CuPc-DPTZ-CMPs/CNT composite in different electrolytes.

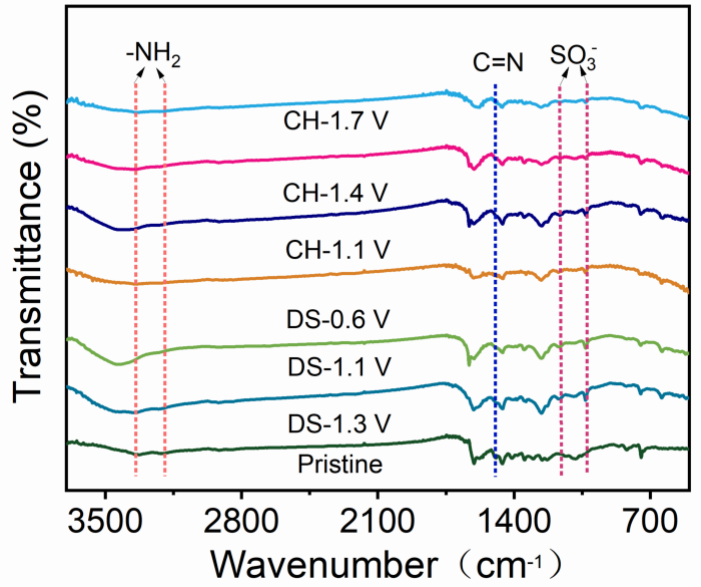


**Fig. S18** Ex situ FT-IR spectra of CuPc-DPTZ-CMPs/CNT composite cathode at the pristine and different (dis)charge states.

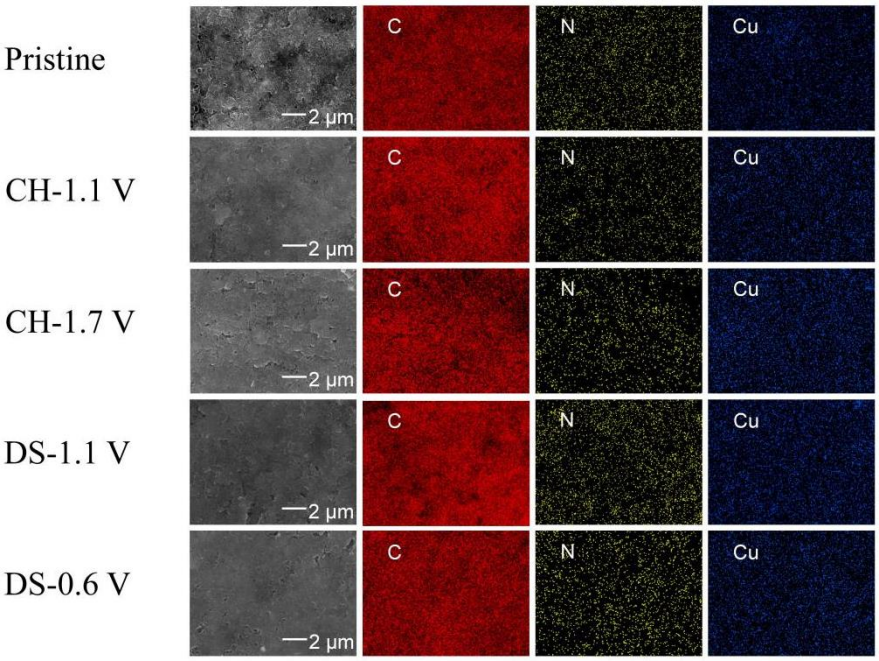


**Fig. S19** SEM images and EDS-mapping of C, N and Cu element distributions on CuPc-DPTZ-CMPs/CNT composite electrodes at different states.

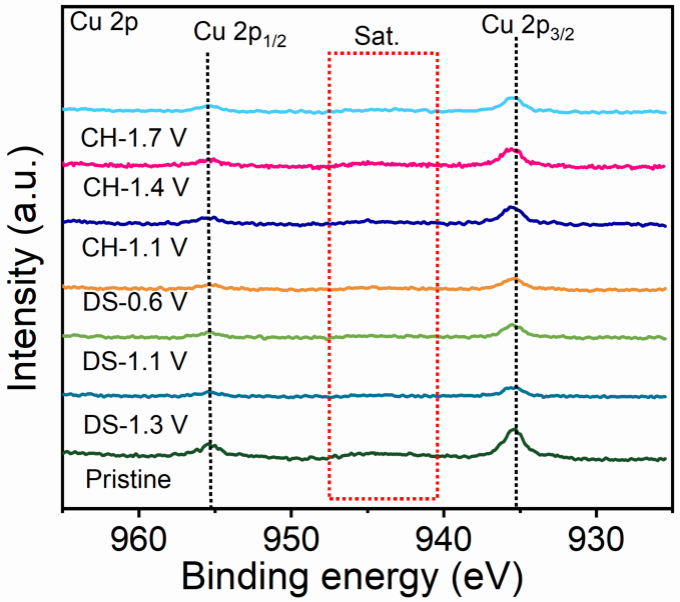


**Fig. S20** Ex situ XPS spectra of Cu 2p at the pristine and (dis)charge states.

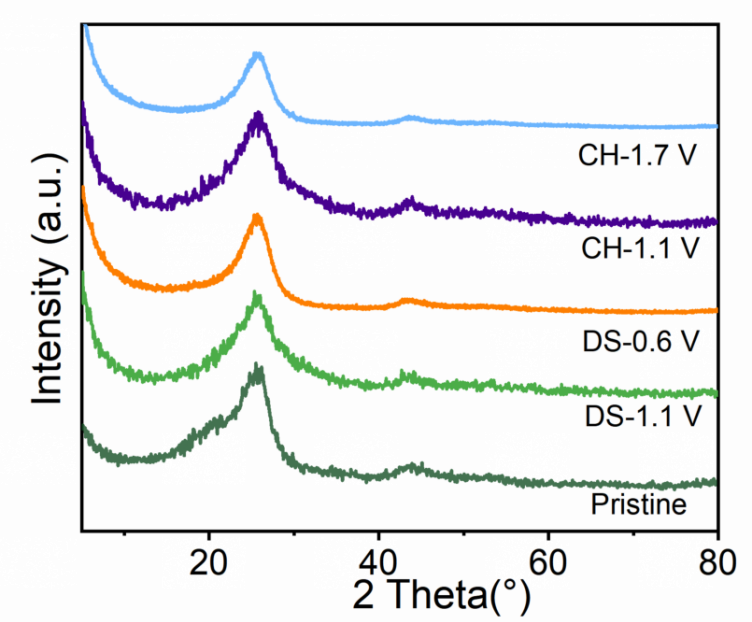


**Fig. S21** Ex situ XRD patterns of CuPc-DPTZ-CMPs/CNT composite cathode at the pristine and (dis)charge states.

# References


[S1] Z. Song, L. Miao, H. Duan, Y. Lv, L. Gan and M. Liu, *Angew. Chem.*, 2024, **136**, e202401049.

[S2] S. Zheng, D. Shi, D. Yan, Q. Wang, T. Sun, T. Ma, L. Li, D. He, Z. Tao and J. Chen, *Angew. Chem., Int. Ed.*, 2022, **61**, e202117511.

[S3] Q. Xu, X. Zhang, X. Yuan, W. Zhang, Y. Li, Y. Zhang and J. Liu, *Adv. Energy Mater.*, 2024, **14**, 2303475.

[S4] Z. Song, L. Miao, H. Duan, L. Ruhlmann, Y. Lv, D. Zhu, L. Li, L. Gan and M. Liu, *Angew. Chem., Int. Ed.*, 2022, **61**, e202208821.

[S5] M. Li, M. Liu, Y. Lu, G. Zhang, Y. Zhang, Z. Li, Q. Xu, H. Liu and Y. Wang, *Adv. Funct. Mater.*, 2024, **34**, 2312789.

[S6] L. Yan, Q. Zhu, Y. Qi, J. Xu, Y. Peng, J. Shu, J. Ma and Y. Wang, *Angew. Chem., Int. Ed.*, 2022, **61**, e202211107.

[S7] N. Wang, Z. Guo, Z. Ni, J. Xu, X. Qiu, J. Ma, P. Wei and Y. Wang, *Angew. Chem., Int. Ed.*, 2021, **60**, 20826–20832.

[S8] J. Xie, F. Yu, J. Zhao, W. Guo, H.-L. Zhang, G. Cui and Q. Zhang, *Energy Storage Materials*, 2020, **33**, 283–289.

[S9] Z. Song, L. Miao, H. Duan, Y. Lv, L. Gan and M. Liu, *Angew. Chem.*, 2024, **136**, e202401049.

[S10] Y. Wang, S. Qiu, D. He, J. Guo, M. Zhao, C. Zheng, X. Wang and C. Wang, *ChemSusChem*, 2023, **16**, e202300658.

[S11] H. Zhang, D. Xu, L. Wang, Z. Ye, B. Chen, L. Pei, Z. Wang, Z. Cao, J. Shen and M. Ye, *Small*, 2021, **17**, 2100902.

[S12] F. Wan, L. Zhang, X. Wang, S. Bi, Z. Niu and J. Chen, *Adv. Funct. Mater.*, 2018, **28**, 201804975.

[S13] Z. Song, Q. Huang, Y. Lv, L. Gan, M. Liu, D. Z. Song, L. Gan and M. Liu, *Angew. Chem., Int. Ed.,* 2024, **64**, e202418237.

[S14] C. Hu, Y. Chen, Z. Song, L. Miao, H. Duan, Y. Lv, L. Xie, M. Liu and L. Gan, *J. Mater. Chem. A,* 2024, **12**, 12818–12825.

[S15] C. Hu, X. Yang, P. Liu, Z. Song, Y. Lv, L. Miao, M. Liu and L. Gan, *J. Mater. Chem. A,* 2024, **12**, 11867–11874.

[S16] T. Shi, C. Hu, Q. Huang, Z. Song, Y. Lv, L. Miao, L. Gan, D. Zhu, Y. Zhang and M. Liu, *Chem. Eng. J.,* 2024, **500**, 157627.

[S17] L. Zhang, Y. Zhang, X. Wang, X. Wang, Q. Wang, J. Li, Z. Li, K. Ding, Y. Peng and H. Liu, *Adv. Funct. Mater.*, 2025, e13189.

[S18] L. Zhang, X. Wang, X. Wang, Q. Wang, J. Li, M. Zhao, K. Ding, H. Liu and Y. Wang, *Chem. Eng. J.*, 2025, **521**, 166985.

[S19] Y. Zhang, C. Zhao, Z. Li, Y. Wang, L. Yan, J. Ma and Y. Wang, *Energy Storage Materials*, 2022, **52**, 386-394.